Realization of Dual Band Pattern Diversity with a CRLH-TL Inspired Reconfigurable Metamaterial

Jiahao Zhang, Sen Yan, *Member, IEEE*, and Guy A. E. Vandenbosch, *Fellow, IEEE*

***Abstract*—A reconfigurable dual band antenna with pattern diversity is proposed. By switching the dispersion curve of a Composite Right/Left Handed Transmission Line (CRLH-TL) inspired structure, the antenna is able to realize both a broadside pattern and an omni-directional pattern in both the 2.4835-2.5 GHz ISM band and the 3.4-3.5 GHz WiMAX band. Despite its complex reconfigurability, only one feeding port is used. A small dual frequency separation ratio is reached, which makes the antenna suitable for low frequency range wireless communication systems. A prototype is fabricated and the measured results agree well with the simulated ones.**

***Index Terms*—Reconfigurable Metamaterials, Reconfigurable Antenna, CRLH-TL, Dual Band, Radiation Pattern.**

I. Introduction

SOME time ago, the use of metamaterials was suggested as an alternative way to boost antenna performance and reduce the size of the radiator [1]-[6]. This suggestion proved to be very successful. Nowadays, reconfigurable metamaterials are drawing a lot of attention since they give the designer an extra set of degrees of freedom for the synthesis of innovative adaptive systems. The unique electromagnetic field manipulation properties enabled by reconfigurable metamaterials make them an attractive solution in a wide set of applicative scenarios [7] including antenna design [8], [9]. Reconfigurability can be achieved by using multiple radiators [10], switching the parasitic elements [11], adjusting the radiator structure [12], etc. This is mostly done in an electric way by using Radio Frequency Micro-Electro-Mechanical Systems (RF MEMS), or mainly PIN diodes and varactors because of the low cost, the simple control strategy, and the ease to be integrated [13]. Note that pattern reconfigurable antennas are very important in many application scenarios such as Wireless Body Area Networks (WBAN) and Multiple Input Multiple Output (MIMO) systems, since they have the potential to avoid the interference of noise sources by redirecting the null position. They also may provide a larger coverage by redirecting the main beam [14], [15]. The monopole-like pattern (omni-directional) and the patch-like pattern (broadside) are frequently combined when realizing pattern diversity [14], [16]-[18]. In WBAN systems, different communication links require different antenna patterns. When two on-body devices communicate, an omni-directional pattern along the body is needed. However, when an on-body device communicates with an off-body device, a broadside pattern is more desirable [19]. In MIMO applications, pattern reconfigurable antennas can be used to increase the system capacity, by reducing the sub-channel correlation or increasing the received signal power [14], [20], [21]. In [14] it turns out that the MIMO system capacity can be improved by using a reconfigurable antenna, with the ability of switching the radiation pattern between a monopole- or patch-like pattern. However, all these antennas that are described in literature only operate in a single band and have a quite complex structure.

CRLH-TL is a subtype of planar metamaterial that can be systematically designed to have both positive and negative phase velocities, which allows antennas to work not only in the positive mode, but also in the zero mode and the negative mode. The use of CRLH-TL can thus be quite beneficial to achieve pattern diversity, since it has the ability to achieve both broadside and omni-directional patterns by working with the different modes. By reconfiguring the dispersion properties, it is possible to choose the resonant mode of the CRLH-TL based radiator in certain frequency bands. Thus by using the CRLH-TL based method, more freedom and flexibility in the design can be obtained compared to other approaches. CRLH-TLs have been used in multiband antennas [22]-[25], and in frequency reconfigurable antennas [26], [27]. Efforts have also been made to utilize CRLH-TL in pattern reconfigurable antennas by reconfiguring the dispersion curve of the CRLH-TL. The antenna in [19] can resonate at the zero mode or the +1 mode, yielding a broadside or an omni-directional radiation pattern. However, the antenna operates in a single band, and its control system was not realized. A CRLH-TL based dual band antenna with pattern diversity was proposed in [28]. However, two ports and two different radiators were used to achieve two

Manuscript received September 8, 2017.

This work was partly supported by the Research Foundation – Flanders (F.W.O.) Postdoctoral Fellowship (No. 12O1217N). (Corresponding author: Sen Yan).

J. Zhang and G. A. E. Vandenbosch are with the ESAT-TELEMIC Research Division, Department of Electrical Engineering, KU Leuven, 3001 Leuven, Belgium (e-mail: jiahao.zhang@esat.kuleuven.be). S. Yan is with the ESAT-TELEMIC Research Division, Department of Electrical Engineering, KU Leuven, 3001 Leuven, Belgium, and also with the School of Electronics and Information Engineering, Xi'an Jiaotong University, Xi'an, Shanxi 710049, China (e-mail: sen.yan@xjtu.edu.cn).

Color versions of one or more of the figures in this communication are available online at http://ieeexplore.ieee.org.

Digital Object Identifier

TABLE I
CHARACTERISTICS OF THE PROPOSED ANTENNA

Switch		Lower band		Higher band	
		Mode	Pattern	Mode	Pattern
State 1	ON	0	Omni-directional	+1	Broadside
State 2	OFF	-1	Broadside	0	Omni-directional

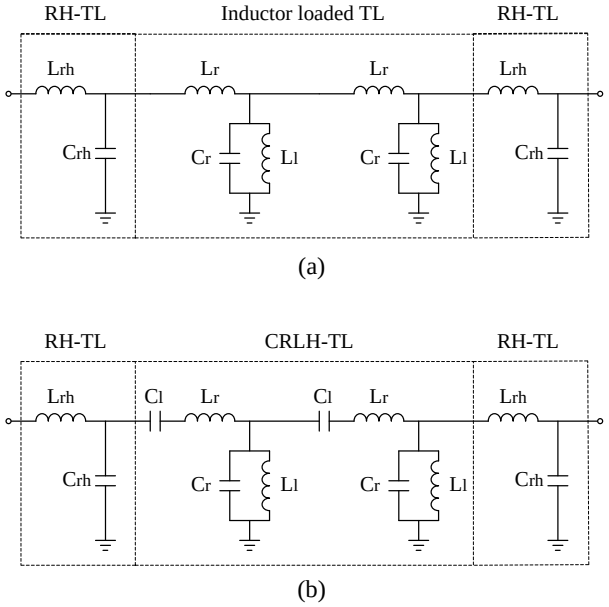

Fig. 1. Equivalent circuit of the resonant structure. (a) state 1: RH-TL embedded with inductor loaded TL, (b) state 2: RH+CRLH+RH-TL.

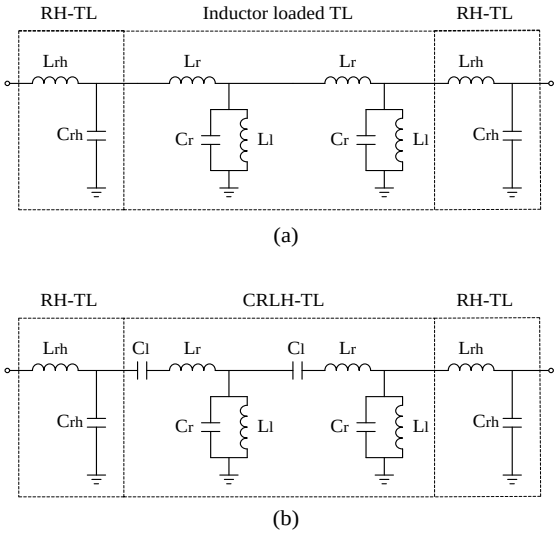

Fig. 2. MSA partially filled with a CRLH structure. The yellow indicates the antenna radiator on a grounded substrate. S1-S6 indicate the switches.

kinds of pattern in a dual band, which makes the antenna quite complicated.

In this paper, a CRLH-TL inspired reconfigurable metamaterial is used in a dual band pattern reconfigurable antenna. The reconfigurable metamaterial structure contains a combination of a CRLH-TL part and an RH-TL part. Switches are used to reconfigure the dispersion properties of the structure.

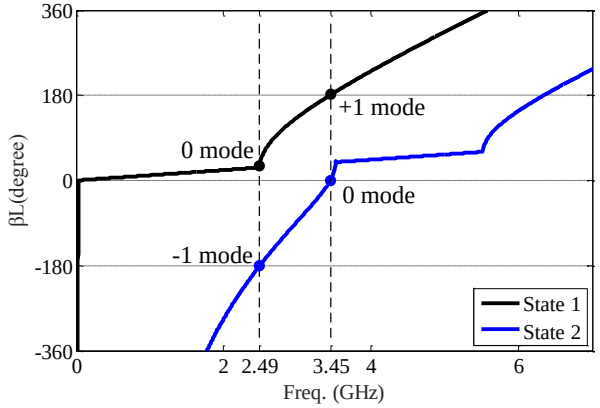

Fig. 3. Dispersion curve of the equivalent circuit. The black line indicates the dispersion curve in state 1 (switches ON), the blue line indicates the dispersion curve in state 2 (switches OFF).

TABLE II
PARAMETER VALUES OF THE EQUIVALENT CIRCUIT

Parameters	State 1	State 2
C_{rh}	0.25 pF	0.25 pF
L_{rh}	0.93 nH	0.93 nH
C_r	3.89 pF	1.95 pF
C_l	N/A	0.47 pF
L_r	1.77 nH	1.77 nH
L_l	1.05 nH	1.05 nH

This structure is applied to an antenna, where mushroom type CRLH cells are partially filling a conventional microstrip radiator. The antenna is able to switch its radiation pattern in the 2.5 GHz ISM band and the 3.5 GHz WiMAX band by reconfiguring the resonant modes, see Table I. A dual band pattern reconfigurable antenna with a single feeding port is achieved. Despite the complex reconfigurability, only one radiator is used, and a simple structured bias network is realized. The electrical size of the proposed antenna is $0.67\times0.67\ \lambda^2$, with a low profile of $0.058\ \lambda$ (λ is the wavelength in free space at the lower operating frequency). The frequency separation ratio is only 1.39. The innovation compared with [19] is that dual band operation is realized, and compared with [28] that a novel structure combining CRLH-TL and RH-TL is proposed, which increases the design freedom.

The organization of this paper is as follows. The operating theory of the CRLH-TL inspired reconfigurable metamaterial is briefly given in section II. The reconfigurable antenna is introduced in section III. Simulations and measurements are discussed in section IV.

II. OPERATING MECHANISM

The propagation constant of a conventional microstrip line is given by:

$$\beta^{RH} = \omega\sqrt{C_{rh}{}'L_{rh}{}'} \quad (1)$$

where $C_{rh}{}'$ and $L_{rh}{}'$ are the capacitance and inductance per unit length. The resonant frequencies of such a conventional

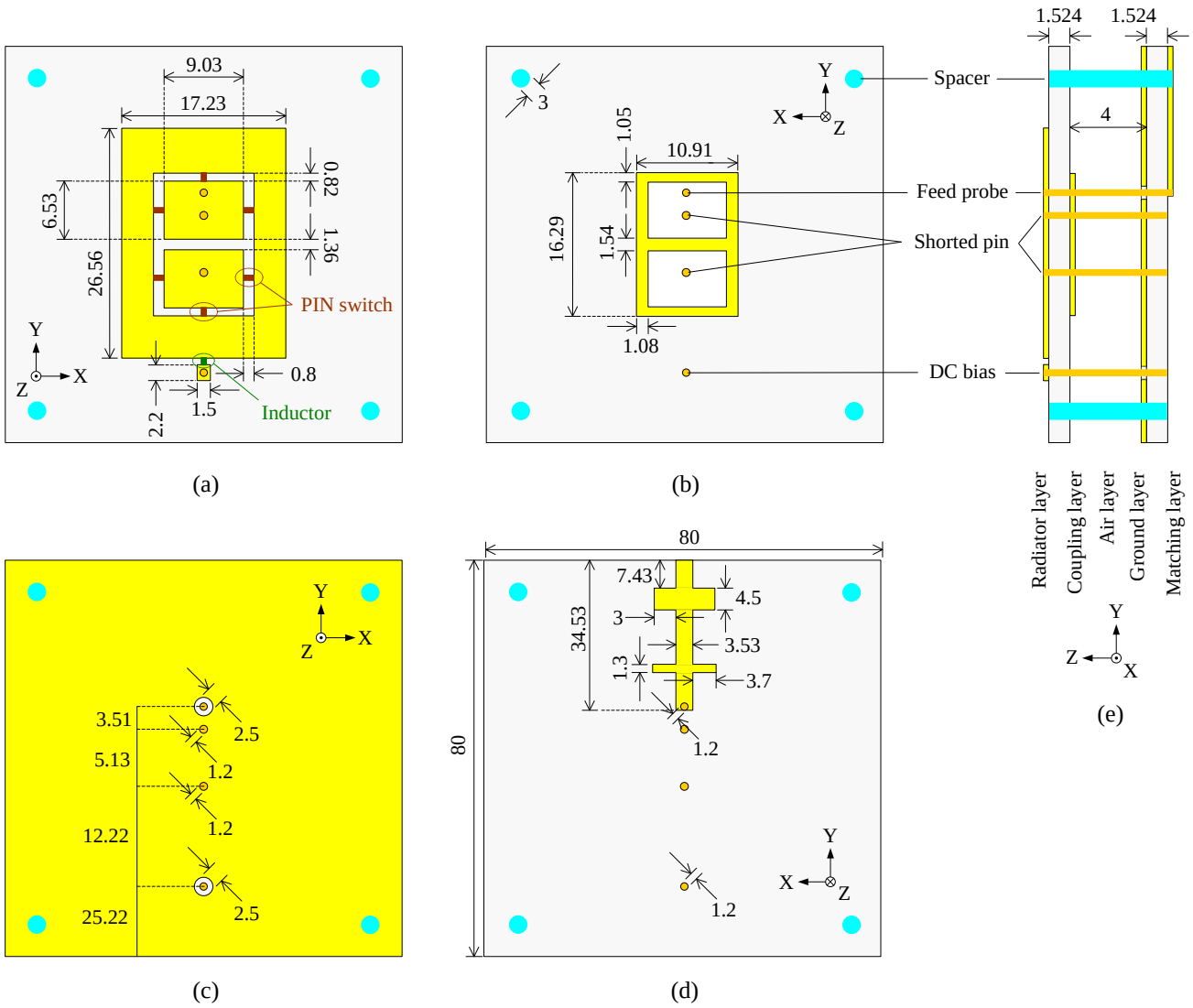

Fig. 4. Topology of the proposed antenna: (a) L1: radiator layer, (b) L2: coupling layer, (c) L3: ground layer, (d) L4: matching layer, (e) side view.

RH-TL of equivalent length d are given by:

$$\beta_n^{RH} \mathrm{d} = \mathrm{n}\pi \tag{2}$$

where n=±1, ±2, … is the resonant index.

A CRLH-TL is composed of a sequence of identical unit cells. The unit cell contains both RH and LH parameters, cascaded along the propagation direction. Considering a CRLH-TL with an RH capacitance of C_r, an RH inductance of L_r, an LH capacitance of C_l, and an LH inductance of L_l, the dispersion relation is given by [29]:

$$\beta \mathrm{p} = \mathrm{s}(\omega)\sqrt{\omega^2 L_r C_r + \frac{1}{\omega^2 L_l C_l} - \left(\frac{L_r}{L_l} + \frac{C_r}{C_l}\right)} \tag{3}$$

where

$$\mathrm{s}(\omega) = \begin{cases} -1 & if\ \omega < \omega_{\tau 1} = \min\left(\frac{1}{\sqrt{L_r C_l}}, \frac{1}{\sqrt{L_l C_r}}\right) \\ 1 & if\ \omega < \omega_{\tau 2} = \max\left(\frac{1}{\sqrt{L_r C_l}}, \frac{1}{\sqrt{L_l C_r}}\right) \end{cases} \tag{4}$$

and p is the length of the unit cell.

Consider now a structure composed of a CRLH-TL of length d_2 and two pieces of conventional RH-TL of length $\mathrm{d}_1/2$. The total length of the structure is thus $\mathrm{L} = \mathrm{d}_1 + \mathrm{d}_2$. The resonant frequencies of this structure satisfy the resonant condition:

$$\beta_n \mathrm{L} = \beta_n^{RH} \mathrm{d}_1 + \beta_n^{CRLH} \mathrm{d}_2 = \beta_n^{RH} \mathrm{d}_1 + \beta_n^{CRLH} \mathrm{pM} = \mathrm{n}\pi \tag{5}$$

where M is the number of CRLH unit cells. In order to get a more detailed physical understanding, circuit models of two versions of this combined structure are given in Fig. 1.

A rectangular microstrip antenna (MSA) can be modeled as an open-ended conventional RH-TL [30]. By using the positive, negative and zero modes of a CRLH-TL, multi frequency antennas have been designed [23], [31]. However, a large frequency separation between the needed positive and negative modes is always observed, which makes this kind of multi frequency antenna not suitable for wireless systems in the low gigahertz range [25].

To overcome these drawbacks and make the antenna suitable for low frequency range wireless communication systems, the first main idea in this paper is to employ a structure which combines both CRLH-TL and RH-TL parts in order to obtain enhanced degrees of freedom in the design and reduce the large frequency separation mentioned above [25]. To achieve the pattern diversity in two bands, the second main idea is to make this structure reconfigurable. Therefore, RF switches are

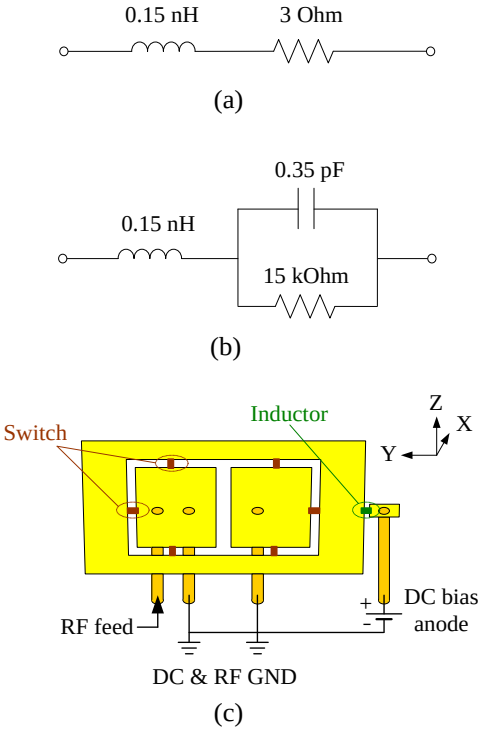

Fig. 5. Equivalent circuit model of the switch in (a) ON state, (b) OFF state. (c) DC bias setup.

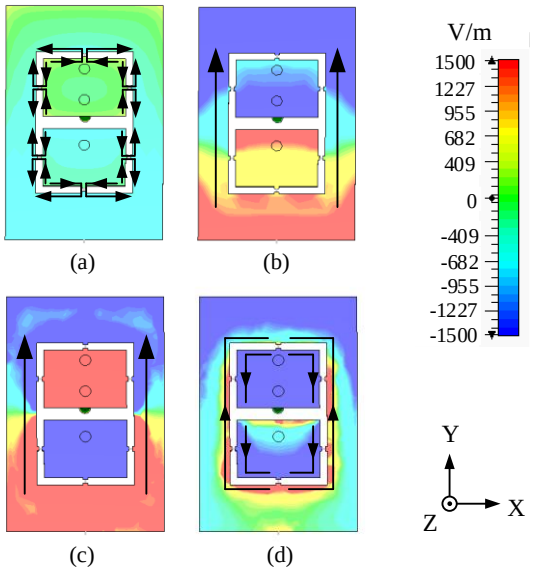

Fig. 6. The Z component of the electric field 1 mm above the antenna. (a) state 1, 2.49 GHz, (b) state 1, 3.45 GHz, (c) state 2, 2.49 GHz, (d) state 2, 3.45 GHz. The arrows show the main direction of the electrical surface current.

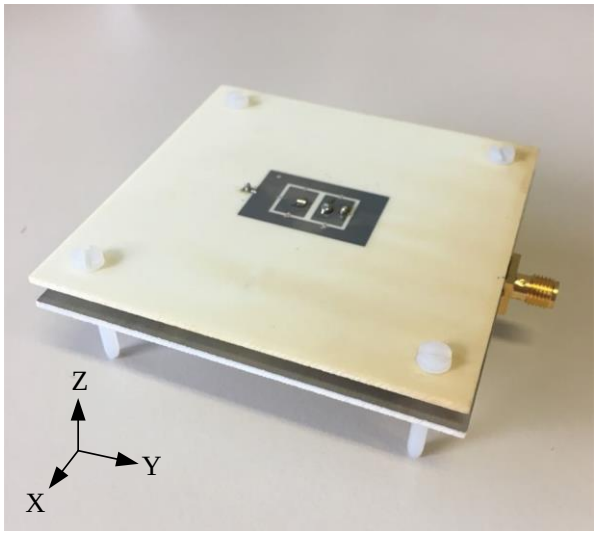

Fig. 7. Prototype of the antenna.

introduced to control the combined structure. By changing the states of the switches, the equivalent parameters of the structure can be tuned, in this way changing the dispersion properties of the CRLH and RH combined TL. This means that the operating modes and the radiation performance in the two bands can be reconfigured. The conjunct using of the RF switches as well as the CRLH-TL and RH-TL combined structure increases the design freedom and makes it possible to accurately control the properties of the antenna simultaneously in two bands with a small frequency separation ratio. This finally allows to reach pattern diversity in two bands.

The proposed antenna is based on a rectangular MSA partially filled with CRLH cells, see Fig. 2. The CRLH-TL cells are implemented with mushroom topologies [32]. The LH inductance (L_l) of the mushroom cells is provided by the shorting pins to the ground and the LH capacitance (C_l) is provided by the gaps between the cells. RF switches are used to connect the partially filled CRLH-TL part and the conventional microstrip part. When all the switches are in the OFF state (state 2), the structure can be described as a RH+CRLH+RH-TL structure, as shown in Fig. 1 (b), which leads to three resonant modes: the +1/-1 modes and the 0 mode, where $C_{rh} = C_{rh}' \cdot d_1/2$, $L_{rh} = L_{rh}' \cdot d_1/2$. When all the switches are in the ON state (state 1), the gaps within the structure are shorted, eliminating the LH capacitances, as shown in Fig. 1 (a). The structure can be described as a RH-TL embedded with an inductor loaded TL (which can be seen also as an epsilon-negative (ENG) metamaterial [33]). As no C_l is present, the structure shows only the 0 and +1 modes.

By switching the status, the values of the parameters of the structure will change, which reconfigures the dispersion curve of the structure and enables the structure to work in different modes in different frequency bands. More in detail, in state 1 the antenna resonates at the 0 mode in the lower band and at the +1 mode in the higher band. In state 2, the antenna resonates at the -1 mode in the lower band and at the 0 mode in the higher band. The +1/-1 modes will result in a broadside radiation pattern, and the 0 mode will result in an omni-directional pattern. In this way, pattern diversity in the two bands is achieved.

The dispersion properties of the whole combined transmission line structure in Fig. 1 are illustrated in Fig. 3. The chosen resonant frequencies are f_0=2.49 GHz and f_1=3.45 GHz in state 1, and f_{-1}=2.49 GHz and f_0=3.45 GHz in state 2. The circuit models were chosen to fit these resonant frequencies. To this goal, formulas (1)-(5) were used. Note that in Fig. 3, the 0

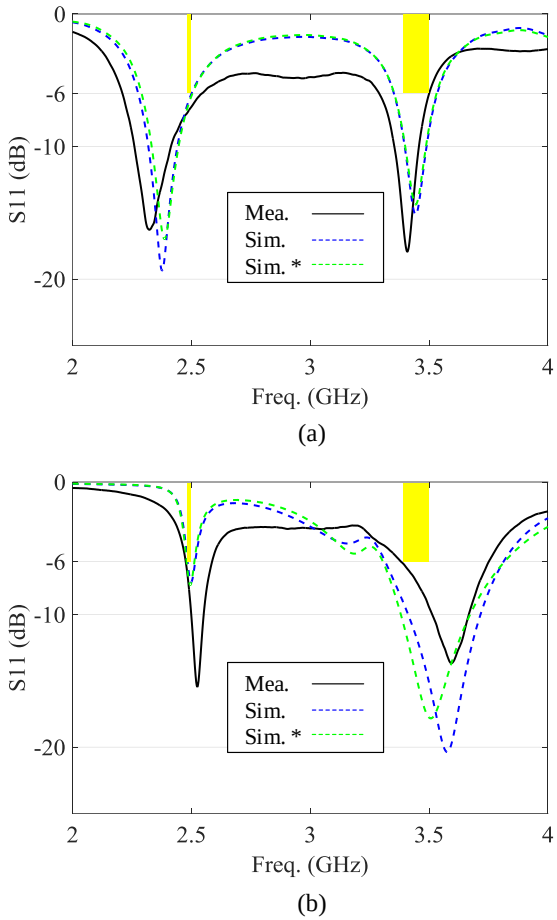

Fig. 8. Reflection coefficients: (a) state 1, (b) state 2. The yellow rectangles indicate the -6 dB 2.4835-2.5 GHz ISM band and the -6 dB 3.4-3.5 GHz WiMAX band, respectively. The simulated Sim.* results (green dashed line) are for the case with ground size 70×70 mm^2.

mode of state 1 is positioned slightly higher than the $\beta L = 0$ axis. This is due to the presence of the RH-TL. The component values obtained are given in Table II. Comparing the two states, it is seen that the RH parameters stay the same. This is because the length and width of the RH-TL parts do not change. The L_r and L_l are mainly related to the length of the CRLH cell and the shorting pin respectively, which also do not change when switching. When the switches are in the ON state, the width of the unit cell of the CRLH-TL becomes larger, and a larger cell area results in a larger C_r.

Note that in this section. the circuit models explained before were used to have a first very rough idea about the required dimensions of the antenna topology involved. We combined this technique with previous experience in order to come up with a first initial design which was fed into the full wave optimiser.

III. Detailed Antenna Design

The targeted two bands are the quite closely separated 2.5 GHz ISM band and the 3.5 GHz WiMAX band. The basic topology of the antenna already has been described in the previous section. Its detailed design started with the design of the reconfigurable CRLH-TL inspired structure. The CRLH-TL

TABLE III
Reflection Coefficient Results

		Measurement	Simulation
State 1	Lower band	2.21-2.54 GHz	2.28-2.50 GHz
	Higher band	3.29-3.50 GHz	3.35-3.53 GHz
State 2	Lower band	2.48-2.59 GHz	2.48-2.52 GHz
	Higher band	3.38-3.75 GHz	3.32-3.81 GHz

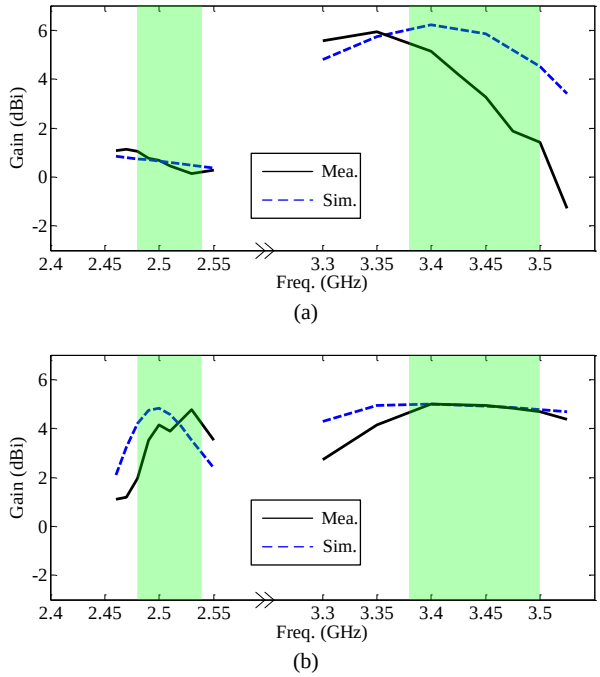

Fig. 10. Realized gain of the antenna. (a) state 1, (b) state 2. The green rectangles indicate the overlapping -6 dB frequency bands of both states, i.e. the operation bands.

was embedded in a common rectangular microstrip antenna. This structure was designed in such a way that the dispersion properties given in Fig. 3 were obtained, see previous section. Note that in order to reach a correct performance, the full wave simulations showed that a coupling structure on the back side of the radiator substrate board is necessary. It is used to enhance the coupling between the cells. An impedance matching network also was designed. An air layer was inserted in the layer structure to increase the bandwidth.

The frequency domain solver in the commercial software CST Microwave Studio was used [34] for all designs. The particle swarm optimization algorithm in CST was used when fine tuning and optimizing the dimensions, including the coupling structure and the impedance matching network.

The detailed design with all dimensions is shown in Fig. 4. It contains two 1.524 mm thick RO4003 substrate layers (permittivity 3.5 and loss tangent 0.0027). The radiator structures (conventional patch and CRLH-TL cells) are located in the top layer (L1) of the upper substrate, while the coupling structure is located in the bottom layer (L2). The ground is located in the top layer (L3) of the lower substrate and the

impedance matching network is located in the bottom layer (L4). Since the equivalent capacitance of a beam lead PIN diode switch in the OFF state is much lower than that of a conventional PIN diode, Skyworks DSM8100-000 beam lead PIN switches were used. Their equivalent circuit models are given in Fig. 5 (a), (b) [35]. Six beam leading diodes (S1-S6) were mounted on top of the radiator to switch the structure. In practice, there is no switch over the central gap between the two cells. This way of working simplifies the bias network, and has a very limited effect on the simulated antenna performance.

The bias network for the switches is depicted in detail in Fig. 5 (c). The DC ground and the antenna ground are connected and form the ground connection for the diode cathodes via the shorting pins. The diode anodes are biased via an RF choke TDK MLK0603L22NJT000 inductor with an inductance of 22 nH and a series resistance of 1 Ohm. When the antenna is in state 1, the switches are forward biased by 1.6 V. When the antenna is in state 2, the bias voltage is 0 V.

IV. Prototype Performance

Fig. 6 shows the simulated vertical component of the electric field 1 mm above the antenna. It is easily observed that in state 1, the E field distribution corresponds to the zero resonant mode at 2.49 GHz and the first positive mode at 3.45 GHz, and that in state 2, the E field distribution corresponds to the first negative mode at 2.49 GHz and the zero resonant mode at 3.45 GHz. The arrows show the main direction of the surface current. It can be seen from Fig. 6 (a) and Fig. 6 (d) that when the antenna works at the zero resonant mode, the surface currents flow mainly around the thin slots, which means currents in opposite directions with a radiation canceling effect in the broadside direction, resulting in an omnidirectional radiation pattern. The patch-like surface currents in Fig. 6 (b) and Fig. 6 (c) result in a broadside radiation pattern.

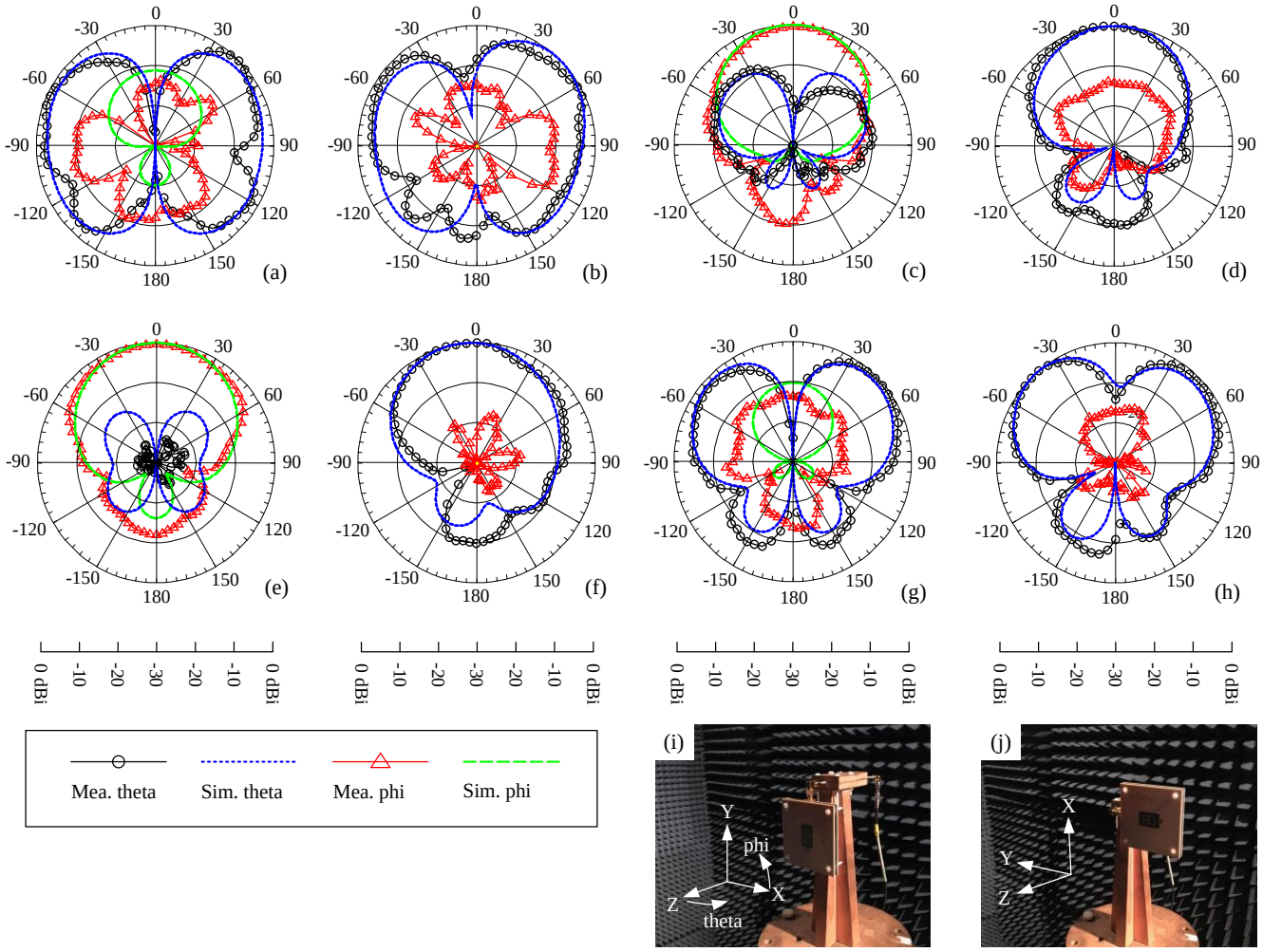

Fig. 9. The normalized radiation patterns of the proposed antenna. State 1 at 2.49 GHz, (a) XZ plane, (b) YZ plane. State 1 at 3.45 GHz, (c) XZ plane, (d) YZ plane. State 2 at 2.49 GHz, (e) XZ plane, (f) YZ plane. State 2 at 3.45 GHz, (g) XZ plane, (h) YZ plane. Radiation pattern measurement setup in (i) XZ plane, (j) YZ plane. The receiving antenna is on the left side of the photos.

An antenna prototype was fabricated, see Fig. 7. The S-parameters of the prototype were measured with an HP 8510 Vector Network Analyzer. The radiation patterns were measured in the anechoic chamber at KU Leuven.

The measured reflection coefficients are compared with the simulated ones in Fig. 8. For both states, the capability of dual

TABLE IV
COMPARISON OF DUAL BAND RECONFIGURABLE ANTENNAS

Ref	Size		Profile		Freq. band	Freq. separation	Reconfigurability
	in λ^2	in mm^2	in λ	in mm	in GHz	ratio	
[45]	1.39×1.31	170×160	N/A	N/A	2.45/5.8	2.37	Pattern
[46]	0.80×0.80	100×100	0.050	6.3	2.4/5.8	2.42	Polarization
[47]	0.76×0.76	100×100	0.024	3.2	2.275/3.95	1.74	Freq.
[48]	0.53×0.53	184×184	0.023	8	0.859/3.45	4.02	Freq.
[49]	0.49×0.46	60×56	0.327	40	2.45/5.25	2.14	Pattern
[50]	0.26×0.26	88×88	0.038	12.5	0.9/1.7	1.89	Freq.
This work	0.67×0.67	80×80	0.058	7.0	2.49/3.45	1.39	Pattern

band operation around 2.5 GHz and 3.5 GHz is clearly shown. The limited bandwidth observed in the lower band of state 2 (-1 mode), is due to the inherently narrow band of the negative mode [23], [25], [36], [37]. The discrepancy between simulations and measurements is due to the dimensional tolerances of the fabrication process and the manual mounting procedure for the switches. The diode switches were manual bonded by conductive glue, which results in a relatively high loss.

Note that the -6 dB criterion (or VSWR 3:1 criterion) is used quite widely to define the impedance bandwidth, for example both in journal papers [38]-[41] and antenna product specification sheets [42], [43]. Table III summarizes the reflection coefficient performance of the antenna. The overlapping -6 dB frequency bands of both states are 2.48-2.54 GHz and 3.38-3.50 GHz. This means that the operating bandwidths in the lower and the higher band are 60 MHz and 120 MHz, respectively. This dual band antenna is thus effectively able to cover the 2.4835-2.5 GHz ISM band and the 3.4-3.5 GHz WiMAX band.

The normalized radiation patterns are given in Fig. 9. The measured results agree well with the simulated ones. It can clearly be seen that in state 1 the antenna has a typical omni-directional pattern at 2.49 GHz and a typical broadside pattern at 3.45 GHz. In state 2 a broadside pattern and an omni-directional pattern are observed at 2.49 GHz and 3.45 GHz, respectively. The cross-polar components are always below or around -10 dB, which is acceptable in most targeted applications. The front-to-back-ratio (FBR) for all the broadside patterns is always larger than 10 dB. Fig. 10 shows the realized gain of the antenna. The simulations and the measurements match well in the higher band for state 1 and in the lower band for state 2. However, an offset is observed in the lower band for state 1 and in the higher band for state 2. This is because of the frequency shift occurring, see also the reflection coefficient results in Fig. 8. The radiation efficiency can be approximated based on the measured radiation patterns in the two principal planes [44]. This yields the values of 72% and 67% at 2.49 GHz and 3.45 GHz in state 1, respectively, and 76% and 98% at 2.49 GHz and 3.45 GHz in state 2, respectively. The corresponding simulated values are 73% and 71% at 2.49 GHz and 3.45 GHz in state 1, respectively, and 81% and 96% at 2.49 GHz and 3.45 GHz in state 2, respectively. The lower efficiencies in state 1 are mainly due to the higher losses in the ON-state switches. In state 2 mainly dielectric losses occur.

A brief comparison of dual band reconfigurable antennas found in literature is given in Table IV. The proposed antenna has a moderate electrical size and a small frequency seperation ratio. Note that a relatively large ground is used in this design to obtain the patch-like broadside radiation pattern. However, simulations show that a further reduction of the size of the ground, e.g., to 70×70 mm^2 (0.58×0.58 λ^2) almost does not change the performance of the antenna, see the S parameter results in Fig. 8.

V. CONCLUSION

In this paper, a novel reconfigurable metamaterial based pattern diversity antenna is proposed, with an electrical size of 0.67×0.67 λ^2, and a low profile of 0.058 λ. It covers the 2.4835-2.5 GHz ISM band and the 3.4-3.5 GHz WiMAX band. The working mechanism is based on reconfiguring the dispersion curve of a structure which contains a combination of a CRLH-TL part and an RH-TL part. The built prototype was shown to be able to switch its radiation pattern from an omni-directional pattern in the lower band and a broadside pattern in the higher band to a broadside pattern in the lower band and an omni-directional pattern in the higher band. This validates our methodology. By combining the CRLH-TL inspired structure and the reconfigurability concept, more freedom and flexiblity in the design are obtained. Note that the concept of controlling the dispersion curve can be extended to other applications such as filter design and resonator design.

REFERENCES

[1] C. Caloz, and T. Itoh, *Electromagnetic Metamaterials: Transmission Line Theory and Microwave Applications*. New York: Wiley, 2005.

[2] T.J. Cui, D. R. Smith, and R. Liu, *Metamaterials: Theory, Design, and Applications*. New York: Springer, 2010.

[3] F. Martin, *Artificial Transmission Lines for RF and Microwave Applications*. New York: Wiley, 2015.

[4] M.A. Antoniades, H. Mirzaei and G. V. Eleftheriades, "Transmission-line based metamaterials in antenna engineering," in *Handbook of Antenna Technologies*. Singapore: Springer, 2016.

[5] S. Yan, P. J. Soh, and G. A. E. Vandenbosch, "Compact all-textile dual-band antenna loaded with metamaterial-inspired structure,"

IEEE Antennas and Wireless Propagation Letters, vol. 14, pp. 1486-1489, 2015.

[6] S. Lim, C. Caloz, and T. Itoh, "Metamaterial-based electronically controlled transmission-line structure as a novel leaky-wave antenna with tunable radiation angle and beamwidth," *IEEE Transactions on Microwave Theory and Techniques*, vol. 52, no. 12, pp. 2678-2690, Dec. 2004.

[7] G. Oliveri, D. H. Werner, and A. Massa, "Reconfigurable electromagnetics through metamaterials—a review," *Proceedings of the IEEE*, vol. 103, no. 7, pp. 1034-1056, Jul. 2015.

[8] H. Cheribi, F. Ghanem, and H. Kimouche, "Metamaterial-based frequency reconfigurable antenna," *Electronics Letters*, vol. 49, no. 5, pp. 315-316, Feb. 2013.

[9] H. Mirzaei, and G. V. Eleftheriades, "A compact frequency-reconfigurable metamaterial-inspired antenna," *IEEE antennas and wireless propagation letters*, vol. 10, pp. 1154-1157, 2011.

[10] S.-J. Shi, and W.-P. Ding, "Radiation pattern reconfigurable microstrip antenna for WiMAX application," *Electronics Letters*, vol. 51, no. 9, pp. 662-664, Apr. 2015.

[11] Y. Juan, W. Che, W. Yang, Z. N. Chen, "Compact pattern-reconfigurable monopole antenna using parasitic strips," *IEEE Antennas and Wireless Propagation Letters*, vol. 16, pp. 557-560, 2017.

[12] I. Lim, and S. Lim, "Monopole-like and boresight pattern reconfigurable antenna," *IEEE Transactions on Antennas and Propagation*, vol. 61, no. 12, pp. 5854-5859, Dec. 2013.

[13] C. G. Christodoulou, Y. Tawk, S. A. Lane, and S. R. Erwin, "Reconfigurable antennas for wireless and space applications," *Proceedings of the IEEE*, vol. 100, no. 7, pp. 2250-2261, Jul. 2012.

[14] P.-Y. Qin, Y. J. Gou, A. R. Weily, and C.-H. Liang, "A pattern reconfigurable U-slot antenna and its applications in MIMO systems," *IEEE Transactions on Antennas and Propagation*, vol. 60, no. 2, pp. 516-528, Feb. 2012.

[15] S. Zhang, G. H. Huff, J. Feng, and J. T. Bernhard, "A pattern reconfigurable microstrip parasitic array," *IEEE Transactions on Antennas and Propagation*, vol. 52, no. 10, pp. 2773–2776, Oct. 2004.

[16] S. H. Chen, J. S. Row, and K. L. Wong, "Reconfigurable square-ring patch antenna with pattern diversity," *IEEE Transactions on Antennas and Propagation*, vol. 55, no. 2, pp. 472–475, Feb. 2007.

[17] W. L. Liu, T. R. Chen, S. H. Chen, and J. S. Row, "Reconfigurable microstrip antenna with pattern and polarization diversities," *Electronic Letters*, vol. 43, no. 2, pp. 77–78, Jan. 2007.

[18] S.-L. S. Yang and K.-M. Luk, "Design a wide-band L-probe patch antenna for pattern reconfigurable or diversity applications," *IEEE Transactions on Antennas and Propagation*, vol. 54, no. 2, pp. 433–438, Feb. 2006.

[19] S. Yan, and G. A. E. Vandenbosch, "Radiation pattern-reconfigurable wearable antenna based on metamaterial structure," *IEEE Antennas and Wireless Propagation Letters*, vol. 15, pp. 1715-1718, 2016.

[20] B. A. Cetiner, E. Akay, E. Sengul, and E. Ayanoglu, "A MIMO system with multifunctional reconfigurable antennas," *IEEE Antennas and Wireless Propagation Letters*, vol. 5, pp. 463–466, 2006.

[21] D. Piazza, N. J. Kirsch, A. Forenza, R. W. Heath, Jr., and K. R. Dandekar, "Design and evaluation of a reconfigurable antenna array for MIMO systems," *IEEE Transactions on Antennas and Propagation*, vol. 56, no. 3, pp. 869–881, Mar. 2008.

[22] W. Cao, B. Zhang, A. Liu, T. Yu, D. Gou, and X. Pan, "Multi-frequency and dual-mode patch antenna based on electromagnetic band-gap (EBG) structure," *IEEE Transactions on Antennas and Propagation*, vol. 60, no. 12, pp. 6007-6012, Dec. 2012.

[23] N. Amani, M. Kamyab, A. Jafargholi, A. Hosseinbeig, and J. S. Meiguni, "Compact tri-band metamaterial-inspired antenna based on CRLH resonant structures," *Electronics Letters*, vol. 50, no. 12, pp. 847-848, Jun. 2014.

[24] S.-C. Chiu, C.-P. Lai, and S.-Y. Chen, "Compact CRLH CPW antennas using novel termination circuits for dual-band operation at zeroth-order series and shunt resonances," *IEEE Transactions on Antennas and Propagation*, vol. 61, no. 3, pp. 1071-1080, Mar. 2013.

[25] F. J. Herraiz-Martinez, V. Gonzalez-Posadas, L. E. Garcia-Munoz, and D. Segovia-Vargas, "Multifrequency and dual-mode patch antennas partially filled with left-handed structures," *IEEE Transactions on Antennas and Propagation*, vol. 56, no. 8, pp. 2527-2539, Aug. 2008.

[26] S. Somarith, H. Kang, and S. Lim, "Frequency reconfigurable and miniaturized substrate integrated waveguide interdigital capacitor (SIW-IDC) antenna," *IEEE Transactions on Antennas and Propagation*, vol. 62, no. 3, pp. 1039-1045, Mar. 2014.

[27] M. S. Khan, A.-D. Capobianco, A. Iftikhar, S. Asif, B. Ijaz, and B. D. Braaten, "A frequency-reconfigurable series-fed microstrip patch array with interconnecting CRLH transmission lines," *IEEE Antennas and Wireless Propagation Letters*, vol. 15, pp. 242-245, 2016.

[28] S. Yan, and G. A. E. Vandenbosch, "Low-profile dual-band pattern diversity patch antenna based on composite right/left-handed transmission line," *IEEE Transactions on Antennas and Propagation*, vol. 65, no. 6, pp. 2808-2815, Jun. 2017.

[29] A. Lai, T. Itoh, and C. Caloz, "Composite right/left-handed transmission line metamaterials," *IEEE microwave magazine*, vol. 5, no. 3, pp. 34-50, Sep. 2004.

[30] J. Zhang, S. Yan, and G. A. E. Vandenbosch, "A miniature feeding network for aperture-coupled wearable antennas," *IEEE Transactions on Antennas and Propagation*, vol. 65, no. 5, pp. 2650-2654, May 2017.

[31] C.-J. Lee, W. Huang, A. Gummalla, and M. Achour, "Small antennas based on CRLH structures: concept, design, and applications," *IEEE Antennas and Propagation Magazine*, vol. 53, no. 2, pp. 10-25, Apr. 2011.

[32] N. Amani, and A. Jafargholi, "Zeroth-order and TM_{10} modes in one-unit cell CRLH mushroom resonator," *IEEE Antennas and Wireless Propagation Letters*, vol. 14, pp. 1396-1399, 2015.

[33] B.-J. Niu, Q.-Y. Feng, and P.-L. Shu, "Epsilon negative zeroth- and first-order resonant antennas with extended bandwidth and high efficiency," *IEEE Transactions on Antennas and Propagation*, vol. 61, no. 12, pp. 5878–5884, Dec. 2013.

[34] Microwave Studio. (2016). *Computer Simulation Technology (CST)*. [Online]. Available: http://www.cst.com/Products/CSTMWS/

[35] M. Shirazi, T. Li, and X. Gong, "Effects of PIN diode switches on the performance of reconfigurable slot-ring antenna," in *2015 IEEE 16th Annual Wireless and Microwave Technology Conference (WAMICON)*, Apr. 2015, pp. 1-3.

[36] C.-J. Lee, K. M. Leong, and T. Itoh, "Composite right/left-handed transmission line based compact resonant antennas for RF module integration," *IEEE Transactions on Antennas and Propagation*, vol. 54, no. 8, pp. 2283-2291, Aug. 2006.

[37] S. Yan, P. J. Soh, and G. A. E. Vandenbosch, "Wearable dual-band composite right/left-handed waveguide textile antenna for WLAN applications," *Electronics Letters*, vol. 50, no. 6, pp. 424-426, Mar. 2014.

[38] Y. Li, Z. Zhang, J. Zheng, Z. Feng, and M. F. Iskander, "A compact hepta-band loop-inverted F reconfigurable antenna for mobile phone," *IEEE transactions on antennas and propagation*, vol. 60, no. 1, pp. 389-392, Jan. 2012.

[39] D. Caratelli, R. Cicchetti, G. Bit-Babik, and A. Faraone, "A perturbed E-shaped patch antenna for wideband WLAN applications," *IEEE Transactions on Antennas and Propagation*, vol. 54, no. 6, pp. 1871-1874, Jun. 2006.

[40] R. Hossa, A. Byndas, and M. E. Bialkowski, "Improvement of compact terminal antenna performance by incorporating open-end slots in ground plane," *IEEE Microwave and Wireless Components Letters*, vol. 14, no. 6, pp. 283-285, Jun. 2004.

[41] M. A. Habib, A. Bostani, A. Djaiz, M. Nedil, M. C. Yagoub, and T. A. Denidni, "Ultra wideband CPW-FED aperture antenna with WLAN band rejection," *Progress In Electromagnetics Research*, vol. 106, pp. 17-31, 2010.

[42] Antenna Products Inc. (2014). *Specification Sheet—WB-5600M Aantenna.* [online]. Available: http://www.antennaproducts.com/wp-content/uploads/2014/04/WB-5600M3pgs.pdf

[43] 2J Antenna Inc. (2015). *Specification Sheet—2JW0124a Multiband Antenna*. [online]. Available: http://www.2j-antennae.com/images/products/2JW0124a.pdf

[44] D. K. John and J. M. Ronald, *Antennas: For All Applications*. Upper Saddle River, NJ, USA: McGraw-Hill, 2002.

[45] M. Nor, S. Rahim, M. Sabran, P. Soh, and G. A. E. Vandenbosch, "Dual-band, switched-beam, reconfigurable antenna for WLAN

applications," *IEEE Antennas and Wireless Propagation Letters,* vol. 12, pp. 1500-1503, 2013.

[46] P.-Y. Qin, Y. J. Guo, and C. Ding, "A dual-band polarization reconfigurable antenna for WLAN systems," *IEEE Transactions on Antennas and Propagation,* vol. 61, no. 11, pp. 5706-5713, Nov. 2013.

[47] A. Khidre, F. Yang, and A. Z. Elsherbeni, "A patch antenna with a varactor-loaded slot for reconfigurable dual-band operation," *IEEE Transactions on Antennas and Propagation,* vol. 63, no. 2, pp. 755-760, Feb. 2015.

[48] Y. B. Jung, "Dual-band reconfigurable antenna for base-station applications," *Electronics Letters,* vol. 46, no. 3, pp. 195-197, Feb. 2010.

[49] C.-H. Ko, I.-Y. Tarn, and S.-J. Chung, "A compact dual-band pattern diversity antenna by dual-band reconfigurable frequency-selective reflectors with a minimum number of switches," *IEEE Transactions on Antennas and Propagation,* vol. 61, no. 2, pp. 646-654, Feb. 2013.

[50] N. Nguyen-Trong, A. Piotrowski, and C. Fumeaux, "A frequency-reconfigurable dual-band low-profile monopolar antenna," *IEEE Transactions on Antennas and Propagation,* vol. 65, no. 7, pp. 3336-3343, Jul. 2017.